

# Suppression of alpha-induced lateral surface events in the COBRA experiment using CdZnTe detectors with an instrumented guard-ring electrode

---

## The COBRA collaboration

J.-H. Arling<sup>a,b</sup> M. Gerhardt<sup>a</sup> C. Gößling<sup>a</sup> D. Gehre<sup>c</sup> R. Klingenberg<sup>a,1</sup> K. Kröninger<sup>a</sup>  
C. Nitsch<sup>a</sup> T. Quante<sup>a</sup> K. Rohatsch<sup>c</sup> J. Tebrügge<sup>a</sup> R. Temminghoff<sup>a,2</sup> R. Theinert<sup>a</sup>  
S. Zatschler<sup>c</sup> K. Zuber<sup>c</sup>

<sup>a</sup>*Technische Universität Dortmund, Lehrstuhl für Experimentelle Physik IV  
Otto-Hahn-Str. 4a, 44221 Dortmund*

<sup>b</sup>*Deutsches Elektronen-Synchrotron DESY  
Notkestrasse 85, 22607 Hamburg*

<sup>c</sup>*Technische Universität Dresden, Institut für Kern- und Teilchenphysik  
Zellescher Weg 19, 01069 Dresden*

*E-mail:* [robert.temminghoff@tu-dortmund.de](mailto:robert.temminghoff@tu-dortmund.de)

**ABSTRACT:** The COBRA collaboration searches for neutrinoless double beta-decay ( $0\nu\beta\beta$ -decay) using CdZnTe semiconductor detectors with a coplanar-grid readout and a surrounding guard-ring structure. The operation of the COBRA demonstrator at the Gran Sasso underground laboratory (LNGS) indicates that alpha-induced lateral surface events are the dominant source of background events. By instrumenting the guard-ring electrode it is possible to suppress this type of background. In laboratory measurements this method achieved a suppression factor of alpha-induced lateral surface events of  $5300^{+2660}_{-1380}$ , while retaining  $(85.3 \pm 0.1)\%$  of gamma events occurring in the entire detector volume. This suppression is superior to the pulse-shape analysis methods used so far in COBRA by three orders of magnitude.

**KEYWORDS:** CZT, CdZnTe, semiconductor detector, coplanar-grid, guard ring, background suppression, surface events

ARXIV EPRINT: [1701.07432](https://arxiv.org/abs/1701.07432)

---

<sup>1</sup>Deceased 24 May 2017

<sup>2</sup>Corresponding author

---

## Contents

<b>1</b>	<b>Introduction</b>	<b>1</b>
<b>2</b>	<b>Guard-ring instrumentation of CdZnTe detectors</b>	<b>2</b>
<b>3</b>	<b>Charge-cloud dynamics of alpha particles</b>	<b>3</b>
<b>4</b>	<b>Predictions from an electric-field calculation</b>	<b>4</b>
<b>5</b>	<b>Experimental setup</b>	<b>6</b>
<b>6</b>	<b>Measurements and results</b>	<b>7</b>
<b>7</b>	<b>Summary and outlook</b>	<b>11</b>

---

## 1 Introduction

The COBRA (CdZnTe **0** Neutrino Double **B**eta **R**esearch **A**pparatus) collaboration [1] searches for neutrinoless double beta-decay ( $0\nu\beta\beta$ -decay) [2]. This decay is forbidden in the Standard Model of particle physics. The quest for lepton-number violation is a main motivation to search for  $0\nu\beta\beta$ -decay. Furthermore, the detection of this process could give information about several general properties of neutrinos like the neutrino mass scale and mass hierarchy. The decay has not been measured yet, limits on the half-life are of the order of  $10^{25}$  yr, depending on the nuclide under study [3–5]. Special experimental techniques are required to measure such rare decays. One crucial issue is the reduction of background events which can mimic the searched-for decay, coining the term ‘low-background experiment’.

The COBRA collaboration operates a demonstrator setup at the Gran Sasso underground laboratory (Italy), technical details can be found in Ref. [6]. The demonstrator consists of 64 CdZnTe coplanar-grid (CPG) semiconductor detectors with the volume of  $1\text{ cm}^3$  each. CdZnTe contains nine nuclides that can undergo double beta-decays:  $^{64}\text{Zn}$ ,  $^{70}\text{Zn}$ ,  $^{106}\text{Cd}$ ,  $^{108}\text{Cd}$ ,  $^{114}\text{Cd}$ ,  $^{116}\text{Cd}$ ,  $^{120}\text{Te}$ ,  $^{128}\text{Te}$  and  $^{130}\text{Te}$ . Due to its high  $Q$ -value of 2 814 keV [7],  $^{116}\text{Cd}$  is the most promising candidate for the COBRA experiment. No significant excess over the estimated background was found which results in half-life limits of about  $10^{21}$  yr for the ground-state to ground-state  $0\nu\beta^-\beta^-$  transitions of  $^{70}\text{Zn}$ ,  $^{114}\text{Cd}$ ,  $^{116}\text{Cd}$ ,  $^{128}\text{Te}$  and  $^{130}\text{Te}$  as documented in Ref. [8]. One conclusion drawn from the operation of the demonstrator is that the main background component stems from alpha-induced lateral surface events. In the current scheme, lateral surface events are identified by analyzing the recorded pulse shapes in the detector; details of this method can be found in Ref. [9].

All detectors used by COBRA feature a guard ring, which is a boundary electrode surrounding the CPG anodes. It is a common method to improve the detector performance, as it leads to a better balanced weighting potential [10] and to a reduction of leakage currents. In the current

configuration, the guard ring is not instrumented and left on a floating potential. Setting a defined potential on a guard-ring structure to suppress surface events was studied in Ref. [11] using Germanium detectors. First measurements have shown that this novel method can be used for the COBRA detectors as well without deteriorating the detector performance significantly [12]. This paper discusses the instrumentation of guard rings for large  $6 \text{ cm}^3$  detectors used for the upgrade of the COBRA demonstrator.

## 2 Guard-ring instrumentation of CdZnTe detectors

In CdZnTe, the product of lifetime and mobility for electrons and holes is different by three orders of magnitude, introducing a strong interaction-depth dependence of the detectors response. To compensate for this effect, the so-called coplanar-grid technology [13] is used in COBRA. It is a single-polarity charge-carrier sensing method, where in this case only the electron signal is read out. In this technique, two anodes are comb-shaped interleaved and are set on a slightly different electric potential, called grid bias (GB). One anode is set to ground potential and referred to as collecting anode (CA) as it collects the generated electrons. The other is set on a negative potential of typically  $-40 \text{ V}$  and is referred to as non-collecting anode (NCA). A bias voltage (BV) of typically  $-1200 \text{ V}$  is applied to the cathode. The detectors discussed in this publication are  $(20 \times 20 \times 15) \text{ mm}^3$  in size with a volume of  $6 \text{ cm}^3$  and a mass of  $36 \text{ g}$ . Their electrodes are configured according to a so-called coplanar quad-grid (CPqG), i.e. four individual CPG structures, rotated against each other by  $90^\circ$ . The whole CPqG structure is surrounded by a common guard ring (GR) which is left on a floating potential in a default configuration. Such a detector, but without a guard-ring electrode, was characterized extensively in Ref. [14]. Details of the electrode design and its dimensions are depicted in Figure 1.

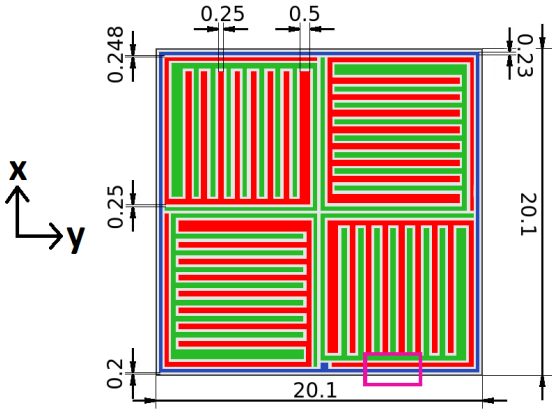


Figure 1. Scheme of the electrode configuration of a CPqG detector. The four sectors comprise individual CPGs, each instrumenting a collecting anode (CA, red) and a non-collecting anode (NCA, green). The surrounding guard ring (GR) is shown in blue. All distances are given in mm. The purple box indicates the position of the detailed view shown in Figure 2.

For the instrumentation of the guard ring a defined potential is set to it, in this case ground potential, which is the same potential as the CA. The guard ring can thus collect charges drifting to it. This is particularly important for charge clouds originating from interactions in the vicinity of the lateral detector surfaces. The anodes and the guard ring are connected to charge sensitive preamplifiers (Cremat CR110<sup>1</sup>). These convert the induced charge signals coming from interactions in the

<sup>1</sup><http://www.cremat.com/CR-110.pdf>

detector volume into voltage signals. The signals are afterwards amplified in linear amplifiers and digitized in flash analog-to-digital converters (FADC SIS3300<sup>2</sup>) with a sampling rate of 100 MHz. The data contains the full pulse-shape information of the measured channels, making it possible to apply pulse-shape analysis tools in the off-line analysis [9]. More details about the data-acquisition can be found in Ref. [6].

The deposited energy in a CPG detector can be reconstructed by calculating the amplitude  $A$  of the difference signal between the CA and NCA signal amplitudes including a so-called weighting factor  $w$ ,

$$E \propto A_{CA} - w \cdot A_{NCA}. \quad (2.1)$$

The weighting factor compensates for effects of electron trapping [13] and can be determined during the calibration process. The energy deposited in each CPqG sector can be reconstructed individually using Equation 2.1. The signal of the guard ring is not considered in the energy reconstruction in this study.

### 3 Charge-cloud dynamics of alpha particles

The aim of this chapter is to roughly estimate the size of the charge cloud based on theoretical calculations to show that from this point of view it is worth to investigate the guard-ring instrumentation for vetoing surface events. The penetration depth of alpha particles from radioactive decays in solids like CdZnTe is very short, about  $R_{\text{initial}} = 20 \mu\text{m}$  for an alpha particle with a kinetic energy of 5 MeV. Therefore, events induced by sources of alpha radiation outside the detector volume deposit their energy in the vicinity of the surfaces and are referred to as lateral surface events. Due to the deposited energy, electron-hole pairs are created at the interaction point. The effect of holes is ignored here because their drift towards the cathode is much slower. The charge cloud of the generated electrons expands while drifting through the detector towards the electrodes due to two main reasons: mutual repulsion of the electrons as well as thermal diffusion. The maximal values for these two quantities can be calculated by considering near-cathode events in the detector. In this case, the created electron cloud drifts through the whole detector volume.

The spread  $\sigma_{\text{diff}}$  of the charge cloud due to diffusion [15] can be calculated as a function of the drift length  $x$  as

$$\sigma_{\text{diff}}(x) = \sqrt{\frac{2k_B T x}{eE}}, \quad (3.1)$$

where  $k_B$  is the Boltzmann constant,  $T$  the absolute temperature,  $e$  the electric elementary charge and  $E$  the electric field strength. To estimate the diffusion and to better compare it with the repulsion, an interval of  $3\sigma$  containing about 99.7% of all charges is used. At room temperature and with an applied BV of  $-1200 \text{ V}$  the resulting charge-cloud expansion due to thermal diffusion for a maximal drift length of 15 mm is

$$R_{\text{diff}}^{\text{max}} = 3\sigma_{\text{diff}}^{\text{max}} = 3\sigma_{\text{diff}}(15 \text{ mm}) \approx 300 \mu\text{m}. \quad (3.2)$$

---

<sup>2</sup><http://www.struck.de/sis3300.htm>

The expansion  $R_{\text{rep}}$  due to mutual repulsion is defined as the largest diameter of the charge cloud contained in a sphere [16]. It can be calculated as function of the drift length to

$$R_{\text{rep}}(x) = \sqrt[3]{\frac{3eNx}{4\pi\epsilon_0\epsilon_r E}}, \quad (3.3)$$

with the number of created charge carriers  $N$  and the permittivity of free space and the relative permittivity,  $\epsilon_0$  and  $\epsilon_r = 10.9$  [17], respectively. As the charges are very close to the detector wall here, they can only expand into a half-sphere. Hence, they are concentrated in a smaller volume. The diffusion is independent from any direction, but for the repulsion one can conservatively estimate the effect by accounting only a half-sphere as containing volume. Therefore, the repulsion can be corrected by the following replacement in Equation 3.3:

$$R_{\text{rep}} \propto \sqrt[3]{\frac{N}{4\pi}} \rightarrow R_{\text{rep}}^{\text{corr}} \propto \sqrt[3]{\frac{N}{2\pi}} \approx 1.25. \quad (3.4)$$

Hence, the value for the repulsion is enlarged by about 25%. The energy of the alpha particles from the  $^{241}\text{Am}$  source is about 5.5 MeV, which is also typical for alpha particles from natural decay chains. In an interaction of this energy, about  $10^6$  charge carriers are produced. Therefore, the resulting expansion due to repulsion is at most

$$R_{\text{rep}}^{\text{corr, max}} = R_{\text{rep}}^{\text{corr}}(15 \text{ mm}) \approx 550 \mu\text{m}. \quad (3.5)$$

The quadratic sum of these two effects and the initial penetration depth can be calculated to estimate an upper limit on the maximal spread  $L_{\text{max}}$  of a charge cloud [18, 19] assuming a maximal drift length of 15 mm for near-cathode events,

$$L_{\text{max}} = \sqrt{(R_{\text{diff}}^{\text{max}})^2 + (R_{\text{rep}}^{\text{corr, max}})^2 + (R_{\text{initial}})^2} \approx 620 \mu\text{m}. \quad (3.6)$$

The effect of the charge-cloud expansion of alpha-induced lateral surface events on the electrodes is shown in Figure 2. The initial interaction has a distance of about 20  $\mu\text{m}$  from the surface. The expansion of the charge cloud is shown after a drift length of 1 mm, 3 mm, 6 mm, 10 mm and 15 mm. Even for the largest drift length of 15 mm, the outermost CPG anode (CA) is not affected by the charge cloud. Hence, a clear separation of alpha-induced lateral surface events and events occurring in the inner detector volume should be possible by instrumenting the guard ring. This is investigated in the following.

#### 4 Predictions from an electric-field calculation

To study the effect of different guard-ring potentials, e.g. floating potential in the default setting or ground potential for enabling charge collection, an electric-field simulation is performed using the simulation tool COMSOL Multiphysics in version 5.2 [20].

The current CPqG detector design is implemented in terms of dimensions and electrode design, the typical material-specific values for CdZnTe are taken from Ref. [21]. The applied bias voltage is assumed to be  $-1200 \text{ V}$  and a typical value of  $-40 \text{ V}$  is chosen for the GB. Configurations with

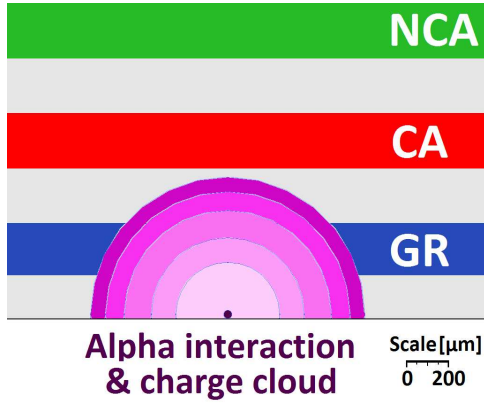


Figure 2. Detailed top view of the anode side as marked in Figure 1. The different types of magenta indicate the expansion of the charge cloud after a drift length of 1 mm, 3 mm, 6 mm, 10 mm and 15 mm. The dark dot highlights the initial charge cloud.

different guard-ring potentials are simulated. In addition, the configuration of the CPqG anodes is varied: if a CA or an NCA bias is applied to the outermost anode, the configuration is referred to as CA<sub>out</sub> and NCA<sub>out</sub> mode, respectively. The simulated electric field-line distribution for the CA<sub>out</sub> mode with the guard ring on ground potential is shown in Figure 3. Here, field lines start on the

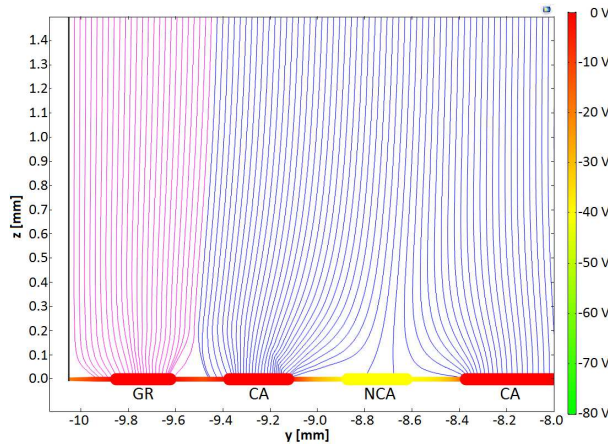


Figure 3. Electric field-line distribution shown in a cross section close to the detector edge. The guard ring is set on ground potential. The chosen GB and BV are  $-40$  V and  $-1200$  V. Field lines ending on the GR are colored in pink, those ending on the CPqG anodes in blue.

cathode in equidistant steps of  $25 \mu\text{m}$  and they end on the different electrodes (GR, CA and NCA as highlighted). Field lines ending on the guard ring are colored in pink in contrast to field lines ending on either of the CPqG anodes, which are shown in blue.

The innermost field line ending on the guard ring starts at a distance of  $625 \mu\text{m}$  from the detector edge. The maximal distance depends on the depth of the starting position, and a slope for the first 2 mm below the anode side is observed before the field lines are almost parallel. Energy deposited between the detector surface and the innermost field line ending on the guard ring will not be detected by the CA. This will lead to a decrease in the overall detection efficiency, but it will in particular suppress a large fraction of alpha-induced lateral surface events, according to Equation 3.6. The area influenced by the instrumented guard ring is visualized in Figure 4. This contour plot depicts the start positions of electric field lines and differentiates between end positions on the guard-ring electrode or the CPqG anodes. The dips in the area influenced by the CPqG at the middle of the sides arise from the transitions between the different CPG sectors. At the bottom, the dip is larger because of the guard-ring contact pad. The ratio of the area influenced by the guard

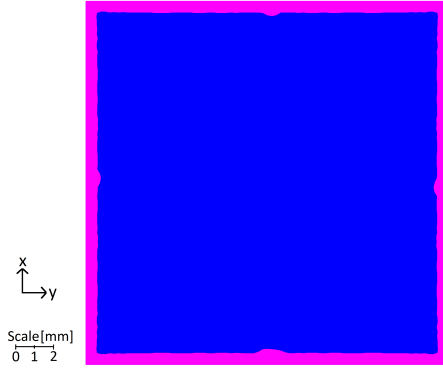


Figure 4. Contour plot of charge collection of the guard ring and the CPqG anodes in  $CA_{out}$  mode as seen from the top. Shown are the projected start positions of field lines finally ending on the guard ring (pink) or on either of the CPqG anodes (blue). The chosen GB is  $-40$  V and BV is  $-1200$  V.

ring relative to the full area is a measure of reduction of the fiducial detector volume,  $\epsilon_{fid}$ . The results for the  $CA_{out}$  mode, as depicted in Figure 4, and for the  $NCA_{out}$  mode are

$$\epsilon_{fid}^{CA_{out}} = 87.7 \% \quad \text{and} \quad \epsilon_{fid}^{NCA_{out}} = 86.0 \%, \quad (4.1)$$

respectively. The uncertainties in these calculations are negligible as the mesh for the numerical calculation is fine ( $25 \mu\text{m}$ ), and small variations of the biases do also not show a notable effect. Only the  $CA_{out}$  mode is evaluated in the following because of the expected larger efficiency than in  $NCA_{out}$  mode. In addition, other beneficial effects like less charge-sharing between the sectors favor this mode [? ].

## 5 Experimental setup

The effect of instrumenting the guard ring in terms of a suppression of alpha interactions from the lateral surfaces is studied in measurements. A prototype CPqG detector with guard ring, produced by Redlen Technologies<sup>3</sup>, is used. During characterization of this test detector, the energy resolution in terms of full-width at half maximum (FWHM) for an incident energy of  $662$  keV of the different CPG sectors is measured. Two of the four sectors have only poor energy resolutions of  $5.0 \%$  and  $7.0 \%$ . Another sector is suffering from leakage currents degrading its performance immensely, while not influencing the other sectors. Finally, the last remaining sector provides a satisfactory energy resolution of  $3.0 \%$ . This sector is therefore chosen as the sector for testing.

A  $^{241}\text{Am}$  source emitting alpha particles with an energy of  $5.5$  MeV is used to provide a sample of alpha-induced surface interactions. The source is pointed directly on the sector under test. Furthermore, the detector can be irradiated with gamma radiation from a  $^{232}\text{Th}$  source with various gamma lines, the highest at an energy of  $2614$  keV. As the low-energy threshold of the measurement is at about  $280$  keV and the detector used here has a side-length of  $2$  cm, photon interactions can take place all throughout its bulk, as even the lowest energy photons considered here have a considerable probability to pass through the detector.

The detector is mounted on a movable stage, so that it is possible to irradiate the detector at first with gamma radiation and afterwards with the alpha source without switching off the biases when exchanging the sources. Hence, the recorded gamma energy spectrum can be used for a

<sup>3</sup><http://redlen.ca/>

common calibration for each configuration. The measurement setup as well as the tested sectors are depicted in Figure 5.

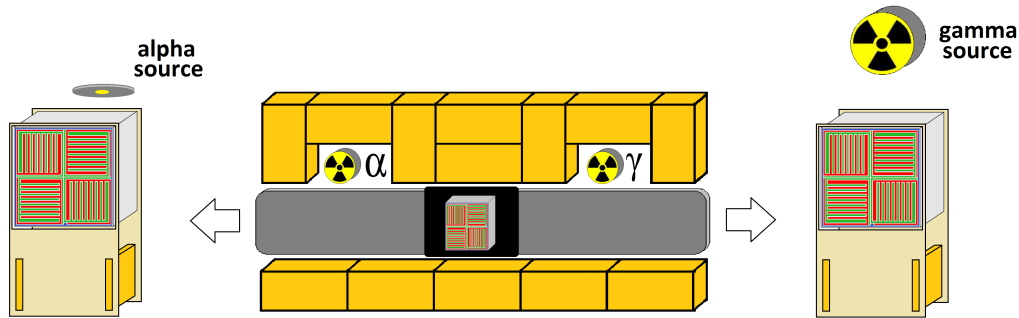


**Figure 5.** Top view of the measurement setup for evaluating the effect of the guard-ring instrumentation. The detector is mounted on a movable stage allowing to shift it between the two different radioactive sources ( $\alpha$ :  $^{241}\text{Am}$  source,  $\gamma$ :  $^{232}\text{Th}$  source). The alpha source is pointed to the sector under test in a distance of approximately 7 mm, whereas the gamma source irradiates the whole detector. The yellow bricks symbolize lead shielding.

To account for background, a dedicated measurement of the background spectrum is performed. The detector is kept in the same position as for an alpha measurement, but the  $^{241}\text{Am}$  source is removed. This background consists mainly of photons emitted by the decay of naturally occurring radioactive isotopes in the laboratory, like  $^{40}\text{K}$ ,  $^{232}\text{Th}$ , or  $^{238}\text{U}$ , cosmic muons and photons scattered from the  $^{232}\text{Th}$ -source, which was present during this measurement to mimic the situation of the alpha measurement as close as possible. Especially at higher energies<sup>4</sup>, muons will be the dominating contribution, as it is known that the activity of internal alpha contaminations is very small (less than 0.5 ppb for U and Th). This has been measured for the bulk material of the detector by Redlen Technologies. Contaminations by  $\alpha$  particles on the surface will lose most of their energy already in the coating of the detectors and will thus not contribute to the high energy part, while it was measured that the coating itself is clean enough to not contribute to the background significantly at this level. As the aim of COBRA is to have a much lower background for the upgrade of the demonstrator setup at the LNGS as it is possible in our laboratory at the surface level, this discussion is only valid for the comparatively high-rate measurements discussed in this publication.

To evaluate the effect of the instrumented guard ring, one measurement is performed with the guard ring on ground potential and one with the guard ring kept on a floating potential. The applied voltages for this measurement campaign are a GB of  $-40\text{ V}$  and a BV of  $-1\,200\text{ V}$ .

## 6 Measurements and results

The energy spectra of the sector under test irradiated with  $^{232}\text{Th}$  gamma radiation are shown in Figure 6. The reconstructed energy spectrum for the case of a floating guard ring is depicted in blue and for the case of an instrumented guard ring in red. The sharp drop around 280 keV stems from the threshold of the energy reconstruction needed for event-by-event triggering. The spectrum

<sup>4</sup>This means basically above the 2614 keV line of  $^{208}\text{Tl}$

shows the typical features of a  $^{232}\text{Th}$  source. The total event rate in the case of an instrumented guard ring is reduced compared to the floating case due to the reduced efficiency. This is expected from the results of the electric-field calculation in [section 4](#). The efficiency shows a slight energy dependence. However, the ratio of the peak contents changes by less than 10 % from 338 keV to 2614 keV. This is also expected, as the lowest energetic photons considered here have a mean free path of about 10 mm and hence, only about 5 % of all interactions will take place in the volume influenced by the guard ring. Consequently, more than 95 % of this radiation interacts in the detector center measured by the CPqG. For higher energetic gamma radiation the fraction of events interacting near the guard ring is even smaller, but as the probability to interact in the bulk of the detector is also reduced, nearly no net effect can be seen in the ratio plot of the two spectra in [Figure 6](#). The constant value of the reduction of the fiducial volume  $\epsilon_\gamma = (85.3 \pm 0.1) \%$  — which will be calculated in [Equation 6.2](#) — is indicated in the plot as a cyan line as well. This shows that while in principle an energy dependence exists, it is so small that it can be neglected here.

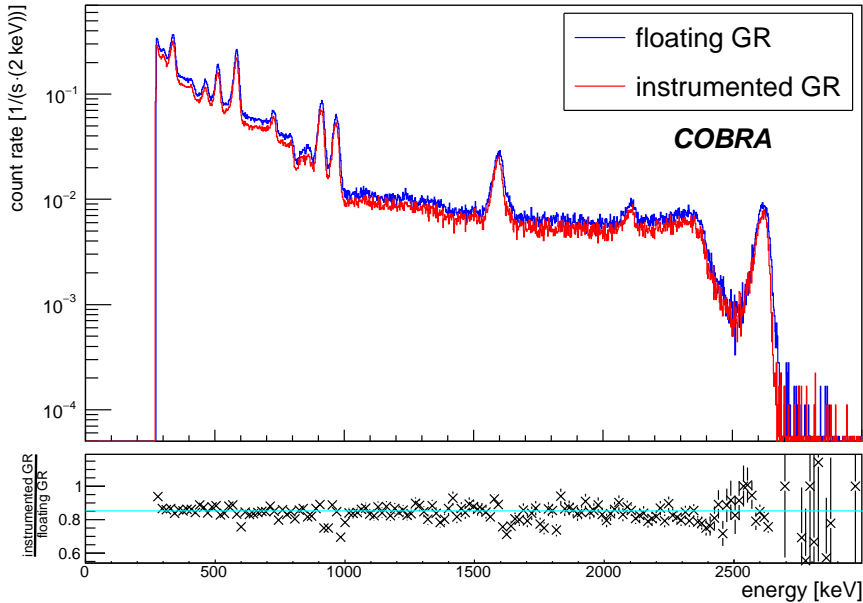


Figure 6. Top:  $^{232}\text{Th}$  energy spectra measured with the sector under test. Shown are the cases of floating (blue) and instrumented guard ring (red). Bottom: Ratio-plot of the two spectra above. The cyan colored constant is the value of  $\epsilon_\gamma$  calculated in [Equation 6.2](#).

For the alpha measurement, the resulting energy spectra for both guard-ring configurations are shown in [Figure 7](#). The unusual spectral shape of the alpha spectrum for the floating guard ring can be explained as follows: The source irradiates the detector uncollimated, otherwise small localized crystal effects like inhomogeneities could affect the results. As the distance between source and detector is only about 7 mm, the path the alpha-particles have to travel until they reach the detector surface is different by up a factor of two due to geometric reasons. Furthermore, the used detectors here are known to have a small dead layer and are coated with an epoxy based resin, which both are not necessarily distributed homogeneously. The same geometric argument as above is also true for the distance the alpha particles have to travel through the lacquer and the dead layer. This results in a smeared distribution shifted towards lower energies. This effect has been verified qualitatively by a Monte-Carlo simulation using GEANT4. For this, a simplified geometry was used and effects by event pile-up, background radiation and energy resolution were neglected, but

the resulting spectral shape showed the same principal features. The interesting point here is that the spectrum of alpha-induced lateral surface events in the instrumented guard-ring configuration is clearly reduced compared to the floating potential case.

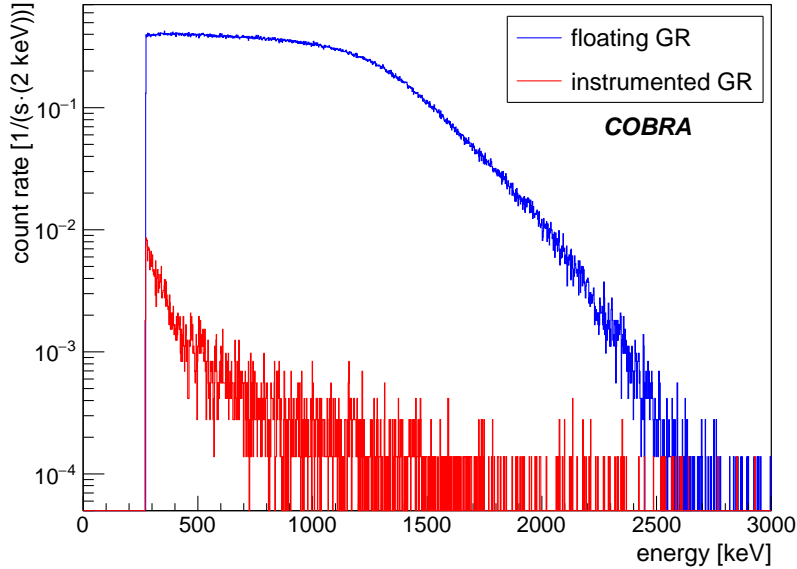


Figure 7.  $^{241}\text{Am}$  energy spectra measured with the sector under test. Shown are the cases of floating (blue) and instrumented guard ring (red).

The spectra resulting from dedicated measurements of the laboratory background are shown in Figure 8. One can see similar spectra for both configurations of the guard ring again. This is expected because most background events stem from gamma radiation and muons. A large fraction of the events in the spectrum from the alpha measurement with an instrumented guard ring (red curve in Figure 7) are caused by laboratory background, which needs to be considered when estimating the suppression of alpha-induced events.

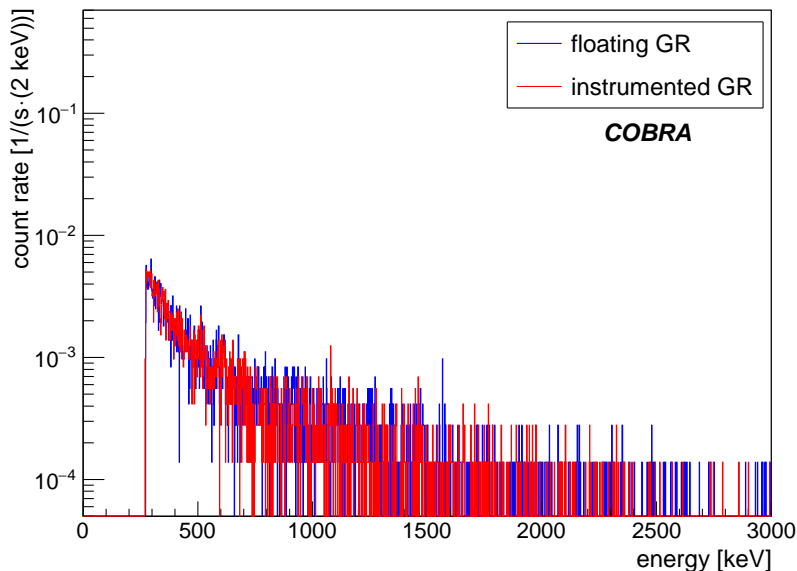


Figure 8. Background energy spectra measured with the sector under test. Shown are the cases of floating (blue) and instrumented guard ring (red).

This is evaluated quantitatively in Table 1 for all six measurements by comparing the count rates,

integrated between 280 keV and 3 000 keV. The quoted uncertainties are due to the statistical Poisson error.

**Table 1.** Results of measurements for sector under test. Given are the integral count rates  $r$  (between trigger threshold and chosen high energy cut-off) in each measurement and for both guard-ring configurations.

		alpha measurement	background measurement	gamma measurement
$r_{\text{floating GR}}$	[1/s]	$208.6 \pm 0.2$	$0.493 \pm 0.008$	$42.33 \pm 0.05$
$r_{\text{instrumented GR}}$	[1/s]	$0.498 \pm 0.008$	$0.465 \pm 0.008$	$36.15 \pm 0.04$

The resulting reduction of the fiducial volume for gamma radiation in the case of an instrumented guard ring is estimated as

$$\epsilon_\gamma = \frac{r_{\text{instrumented GR}}^\gamma - r_{\text{instrumented GR}}^{\text{bkg}}}{r_{\text{floating GR}}^\gamma - r_{\text{floating GR}}^{\text{bkg}}}. \quad (6.1)$$

Using the numbers in [Table 1](#), this yields

$$\epsilon_\gamma = (85.3 \pm 0.1) \%. \quad (6.2)$$

This value is comparable with the prediction of  $\epsilon_{\text{fid}} = 87.7 \%$  from the calculation of the electric field ([Equation 4.1](#)). The relative difference between the calculated and the measured value is 2.7%, which is larger than the difference expected due to purely statistical reasons. Instead, the difference arises from effects of a real detector that are not incorporated in the electric-field calculation, e.g. inhomogeneities in the detector bulk, uncertainties in the electrode placements or the energy resolution. The simulation did also not take into account the effect of multiple scattering of high energetic photons in the detector, which in principle leads to a slightly higher chance for an interaction to take place in the volume affected by the guard ring.

The suppression factor for alpha-induced lateral surface events  $\text{SF}_\alpha$  can be defined as

$$\text{SF}_\alpha = \frac{r_{\text{floating GR}}^\alpha - r_{\text{floating GR}}^{\text{bkg}}}{r_{\text{instrumented GR}}^\alpha - r_{\text{instrumented GR}}^{\text{bkg}}}. \quad (6.3)$$

As the rates in the numerator and the denominator differ by about four orders of magnitude, common Gaussian uncertainty propagation cannot be used for the calculation of the ratio. Instead, the suppression factor is estimated based on a toy Monte-Carlo study:  $10^7$  pairs of random numbers are drawn from two Gaussian distributions, characterized by the numerator and the denominator, and the resulting frequency distribution of the ratios of these numbers is interpreted as the probability density of  $\text{SF}_\alpha$ . Because this asymmetric distribution features a strong non-Gaussian tail towards larger values, the suppression factor is estimated by the mode of the distribution. The smallest interval containing 68.3 % of all entries is interpreted as the uncertainty interval. This yields

$$\text{SF}_\alpha = 5300_{-1380}^{+2660}. \quad (6.4)$$

This is a large improvement compared to the pulse-shape analysis currently used to suppress lateral surface events in COBRA [8, 9]: the relative detection efficiency for gamma radiation is about the same, but the suppression factor for alpha-induced lateral surface events is nearly three orders of magnitude larger.

The main region of interest for COBRA is around the  $Q$ -value of  $^{116}\text{Cd}$  at 2614 keV. The suppression factor for alpha-induced lateral surface events is calculated here only up to about 2.5 MeV for the reasons discussed above. However, no deterioration of this factor is expected for higher energies. The charge cloud of a typical alpha particle with an energy of 5 MeV should not reach the inner detector volume. The expansion of the charge cloud of a hypothetical alpha particle with an energy of 10 MeV, which is a little more than the prominently occurring natural energies of alpha radiation can be estimated analog to [section 3](#) to be maximally 750  $\mu\text{m}$  for an interaction close to the cathode. This charge cloud could reach into the CPqG volume in the detector center partly. But even this is no drawback to this method, as this type of events could be vetoed in a coincidence analysis easily, as energy is deposited in the guard ring and the CPqG-area at the same time.

## 7 Summary and outlook

The COBRA collaboration searches for neutrinoless double beta-decay and hence background reduction is a crucial issue. Alpha-induced lateral surface events are the main background source when operating the COBRA demonstrator. In this paper, dedicated laboratory measurements and calculations of electric fields are used to demonstrate that instrumenting the guard ring of CPqG detectors leads to a suppression factor for alpha-induced lateral surface events of  $5300^{+2660}_{-1380}$ , while the reduction of fiducial volume for gamma events occurring throughout the entire detector volume is  $(85.3 \pm 0.1)\%$ .

This concept will be followed in the upgrade of the COBRA extended demonstrator (XDEM). Under optimal conditions and the assumption that the background is dominated by alpha events, the overall background rate is expected to be lowered by two orders of magnitude.

The signals of the guard ring are measured, but not included in the analysis presented here. A modified event reconstruction including the guard-ring signal can in principle be performed. Preliminary studies indicate that using this additional information is feasible and can improve the detector performance (e.g. the detection efficiency) and the veto capabilities for lateral surface events even further.

## Acknowledgments

We thank the LNGS for the continuous support of the COBRA experiment. COBRA is supported by the German Research Foundation DFG (ZU 123/15-1 / GO 1133/3-1). Furthermore, we thank COMSOL for support with the COMSOL Multiphysics simulation and O. Schulz for technical support with the DAQ.

## References

- [1] K. Zuber. COBRA: Double beta decay searches using CdTe detectors. *Phys. Lett. B*, 519:1–7, 2001.

- [2] W. H. Furry. On Transition Probabilities in Double Beta-Disintegration. *Phys. Rev.*, 56:1184, 1939.
- [3] M. Agostini et al. Limit on Neutrinoless Double Beta Decay of  $^{76}\text{Ge}$  by GERDA. *Phys. Procedia*, 61:828–837, 2015.
- [4] K. Asakura et al. Results from KamLAND-Zen. *AIP Conf. Proc.*, 1666:170003, 2015.
- [5] C. Alduino et al. Analysis techniques for the evaluation of the neutrinoless double- $\beta$  decay lifetime in  $^{130}\text{Te}$  with the CUORE-0 detector. *Phys. Rev. C*, 93:045503, 2016.
- [6] J. Ebert et al. The COBRA demonstrator at the LNGS underground laboratory. *Nucl. Instrum. Meth. A*, 807:114–120, 2016.
- [7] S. Rahaman et al. Double-beta decay Q values of  $^{116}\text{Cd}$  and  $^{130}\text{Te}$ . *Phys. Lett. B*, 703:412–416, 2011.
- [8] J. Ebert et al. Results of a search for neutrinoless double- $\beta$  decay using the COBRA demonstrator. *Phys. Rev. C*, 94:024603, 2016.
- [9] M. Fritts et al. Pulse-shape discrimination of surface events in CdZnTe detectors for the COBRA experiment. *Nucl. Instrum. Meth. A*, 749:27–34, 2014.
- [10] Z. He et al. Coplanar grid patterns and their effect on energy resolution of CdZnTe detectors. *Nucl. Instrum. Meth. A*, 411(1):107–113, 1998.
- [11] A. Broniatowski et al. A new high-background-rejection dark matter Ge cryogenic detector. *Phys. Lett. B*, 681(4):305–309, 2009.
- [12] J. Tebrügge. *Commissioning of the COBRA demonstrator and investigation of surface events as its main background*. PhD thesis, TU Dortmund, 2016. arXiv: 1609.03783.
- [13] P. N. Luke. Single-polarity charge sensing in ionization detectors using coplanar electrodes. *Appl. Phys. Lett.*, 65(22):2884–2886, 1994.
- [14] J. Ebert et al. Characterization of a large CdZnTe detector with a coplanar quad-grid design. *Nucl. Instrum. Meth. A*, 806:159–168, 2016.
- [15] Knoll, G. F. *Radiation Detection and Measurement, 4th ed.* John Wiley and Sons, 2010.
- [16] E. Gatti et al. Dynamics of electrons in drift detectors. *Nucl. Instrum. Meth. A*, 253(3):393–399, 1987.
- [17] Capper, P. *Properties of narrow gap cadmium based compounds*. Institution of Engineering and Technology, 1994.
- [18] B. Donmez et al. Continued studies of single-sided charge-sharing CZT strip detectors. In *IEEE Nucl. Sci. Symp. Conf. Rec.*, volume 3, pages 1408–1411, 2005.
- [19] M. Benoit and L. A. Hamel. Simulation of charge collection processes in semiconductor CdZnTe  $\gamma$ -ray detectors. *Nucl. Instrum. Meth. A*, 606(3):508–516, 2009.
- [20] COMSOL Inc. COMSOL Multiphysics. <http://www.comsol.com/>. Online source; accessed 11-December-2016.
- [21] Q. Zhang et al. Progress in the Development of CdZnTe Unipolar Detectors for Different Anode Geometries and Data Corrections. *Sensors*, 13(2):2447, 2013.